Assessment of the ASCAT wind error characteristics by global dropwindsonde observations

Kun-Hsuan Chou,[1] Chun-Chieh Wu,[2] and Shu-Zheng Lin[1]

Received 19 November 2012; revised 5 August 2013; accepted 7 August 2013; published 29 August 2013.

[1] This research focuses on assessing the accuracy of the advanced scatterometer (ASCAT) wind vector around tropical cyclones by using data from dropwindsondes deployed by the surveillance and reconnaissance flights during 2007–2010. There are 987 matching samples for the comparisons, with wind speed up to 50 m s^{-1}. The bias and root-mean-square differences of wind speed between ASCAT and dropwindsonde data are −1.7 and 5.3 m s^{-1}, respectively. Further analyses also indicate that large wind direction differences occur in the low wind speed regime, while large wind speed differences occur in the high wind speed regime. The accuracy of wind vector in weak wind speed and high wind speed regimes are significantly reduced in saturated regions, implying that the rain contamination issue still affects the accuracy of ASCAT wind retrieval. The wind vector in the medium wind speed regime has much better quality, in good agreement with the satellite's designed specification. The ASCAT wind data obviously contain negative wind speed bias, which grows larger as wind speed increases. A regression fit between ASCAT and dropwindsonde wind speed is adopted to correct the bias of the ASCAT wind speed. The error characteristics are largely determined by the magnitude of wind speed and moisture saturation which are highly variable around the storm. Nevertheless, results from this study suggest that ASCAT wind data of velocities measuring between 12 and 18 m s^{-1} are more reliable and can be applied to determine the radius of 34 knot winds, a critical parameter in operational tropical cyclone analysis.

Citation: Chou, K.-H., C.-C. Wu, and S.-Z. Lin (2013), Assessment of the ASCAT wind error characteristics by global dropwindsonde observations, *J. Geophys. Res. Atmos.*, *118*, 9011–9021, doi:10.1002/jgrd.50724.

1. Introduction

[2] Since the Quick Scatterometer (QuikSCAT) mission ended in November 2009, the advanced scatterometer (ASCAT) launched in October 2006 has become one of the key satellite scatterometers, and since then, validating the accuracy of ocean surface wind vector data from ASCAT has become an important issue. *Bentamy et al.* [2008] examined the accuracy of ASCAT wind observations through comparison with collocated measurements from buoys and QuikSCAT. The comparison between the ASCAT data and buoys indicated that the wind speeds and directions derived from ASCAT agree well with the buoy data. The root-mean-square (RMS) differences of the wind speed and direction are less than 1.72 m s^{-1} and 18°, respectively. However, it was found that the ASCAT wind data have a slightly negative bias of about 0.5 m s^{-1} in high wind speed conditions (above 10 m s^{-1}). The comparison between the ASCAT and QuikSCAT data also showed that for higher wind speed conditions, ASCAT has low bias, and the ASCAT underestimation with respect to QuikSCAT wind data increases with wind speed.

[3] To evaluate the accuracy of the scatterometer wind data, several studies have been performed to compare QuikSCAT wind data against surface buoy data [*Freilich and Dunbar*, 1999; *Ebuchi et al.*, 2002; *Pickett et al.*, 2003]. All these studies demonstrated that the RMS differences between the scatterometer and buoy data were within the satellite's designed specifications for both wind speed (±2 m s^{-1}) and direction (±20°) [*Pickett et al.*, 2003]. Although the above studies have demonstrated the accuracy of wind data derived from QuikSCAT in a variety of applications, their accuracy in heavily precipitating regimes such as tropical cyclones (TCs) is reduced due to the contamination in backscattering [*Brennan et al.*, 2009]. The effects of rain, resolution, and signal saturation would affect the confidence level of operational forecasters in determining the TC wind speed [*Brennan et al.*, 2009; *Weissman and Bourassa*, 2011; *Weissman et al.*, 2012].

[4] Early studies of scatterometer observations and validation by aircraft observations over TCs were accomplished by Seasat-A satellite scatterometer (SASS) in *Hawkins and Black* [1983] and *Black et al.* [1985]. Based on 50 matching samples of SASS-derived wind speeds with surface truth value, *Hawkins and Black* [1983] and *Black et al.* [1985]

[1]Department of Atmospheric Sciences, Chinese Culture University, Taipei, Taiwan.
[2]Department of Atmospheric Sciences, National Taiwan University, Taipei, Taiwan.

Corresponding author: K.-H. Chou, Department of Atmospheric Sciences, Chinese Culture University, 55, Hwa-Kang Rd., Yang-Ming-Shan, Taipei 111, Taiwan. (zkx@faculty.pccu.edu.tw)

2169-897X/13/10.1002/jgrd.50724

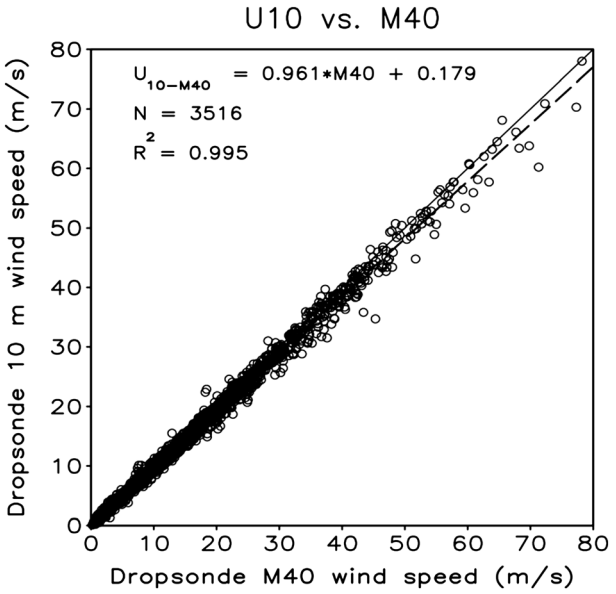

Figure 1. Scatter diagram of wind speed with the linear regression fit line for the 10 m wind speed (U10) and an averaged surface-to-40 m wind speed (M40).

showed that the RMS error of non-rain-contaminated wind vector was 0.8 m s^{-1} for wind speed and 11° for wind direction and that of rain-contaminated wind data revealed larger errors of 1.6 m s^{-1} and 18.5°. Recently, the accuracy of QuikSCAT wind vectors in the environment of TCs was examined via comparison with Global Positioning System (GPS) dropwindsonde winds from Dropwindsonde Observations for Typhoon Surveillance near the Taiwan Region (DOTSTAR) [*Wu et al*., 2005, 2007] missions during 2003–2007 [*Chou et al*., 2010]. The results indicated that the RMS difference between the non-rain-flagged QuikSCAT and dropwindsonde wind data is 2.6 m s^{-1} (17°) for wind speed (direction). Moreover, further analyses showed that QuikSCAT wind data below tropical storm wind strength (17.2 m s^{-1}) are reliable as one useful parameter in determining TC structure.

[5] Following the work from *Chou et al*. [2010], a comparison between ASCAT wind data and equivalent wind observations from the GPS dropwindsondes is conducted for TCs over the Pacific and Atlantic Oceans in this study. These tropospheric soundings include data acquired from DOTSTAR, National Oceanic and Atmospheric Administration/Hurricane Intensity Forecasting Experiment (NOAA/IFEX) [*Aberson and Franklin*, 1999; *Aberson*, 2010; *Rogers et al*., 2006, 2013] during 2007–2010, The Observing System Research and Predictability Experiment-Pacific Asian Regional Campaign (T-PARC) [*Chou et al*., 2011; *Elsberry and Harr*, 2008; *Parsons et al*., 2008; *Chen et al*., 2011; *Huang et al*., 2012; *Wu et al*., 2012a, 2012b] in 2008, and Impacts of Typhoons on the Ocean in the Pacific (ITOP) [*Hawkins and Velden*, 2011; *D'Asaro et al*., 2011] in 2010. The goals of this study are to validate the ASCAT wind vector around TC against dropwindsonde data and to analyze the error characteristics under different TC wind and moisture conditions. More collocated samples can be expected between ASCAT and dropwindsonde data in higher wind speed regions because these dropwindsondes are mostly deployed around the TC. ASCAT data are useful in estimation of the 34 knot wind radius. Moreover, the results of error characteristics can also provide useful information on accuracy of satellite-derived wind products, especially in TCs, which is helpful for the operational TC analysis and for initializing numerical forecast models.

[6] In section 2, the data and techniques used to identify the rain-contaminated samples are described. Results for different wind speed regimes, moisture condition, portion of storms, and bias correction are provided in section 3, followed by discussions and conclusions in sections 4 and 5, respectively.

2. Data and Methodology

[7] ASCAT is one of the instruments carried on board the meteorological operational polar satellites launched by the European Space Agency and operated by the European Organisation for the Exploitation of Meteorological Satellites (EUMETSAT). ASCAT is an active microwave sensor designed to retrieve ocean surface wind data. The mission of ASCAT is to enhance the spatial and temporal resolution of surface wind observations at global and regional scales. ASCAT is designed with two sets of three antennas which are used to generate radar beams on both sides of the satellite ground track. These beams illuminate approximately 550 km wide swaths (separated by about 700 km) as the satellite moves along its orbit, and each provides measurements of radar backscatter from the sea surface on a 25 or 12.5 km grid. For the Satellite Application Facility on Ocean and Sea Ice and the advanced scatterometer of EUMETSAT Advanced Retransmission Service wind products, the C-band geophysical model function (CMOD5.N) for calculating equivalent neutral winds is applied [*Hersbach et al*., 2007; *Verhoef et al*., 2008]. More detailed information about the ASCAT wind products can be found in the ASCAT Wind Product User Manual (www.knmi.nl/scatterometer). The ASCAT orbit data are obtained from the Royal Netherlands Meteorological Institute (KNMI) website, with a resolution of 25 km during 2007–2009 and of 12.5 km in 2010.

[8] Global Positioning System (GPS) dropwindsondes designed by the National Center for Atmospheric Research are applied for validating the ASCAT wind vector. The dropwindsondes are designed with a near-surface fall rate of 10 m s^{-1} and a sampling rate of 2 Hz, thus providing approximately 5 m vertical resolution measurements in the lower troposphere. Note that newer dropwindsondes are designed with a sampling rate of 4 Hz since 2010. The estimated typical measurement errors in the wind speed are 0.5–2.0 m s^{-1} [*Hock and Franklin*, 1999]. Therefore, the dropwindsonde measurements provide good quality wind observations for validating the scatterometer-retrieved wind data. The data set used for the validation in this study consists of 7142 atmospheric sounding profiles obtained from dropwindsondes in four different programs (DOTSTAR, NOAA/IFEX, T-PARC, and ITOP) during 2007–2010.

[9] Although the GPS dropwindsonde has a sampling interval of 0.25 or 0.50 s, not all the dropwindsondes directly measure the 10 m wind (U_{10}). In order to obtain a larger sampling database by including cases with missing surface wind measurements, the surface-to-40 m averaged wind speed (M40) is calculated and used to estimate U_{10} based on a

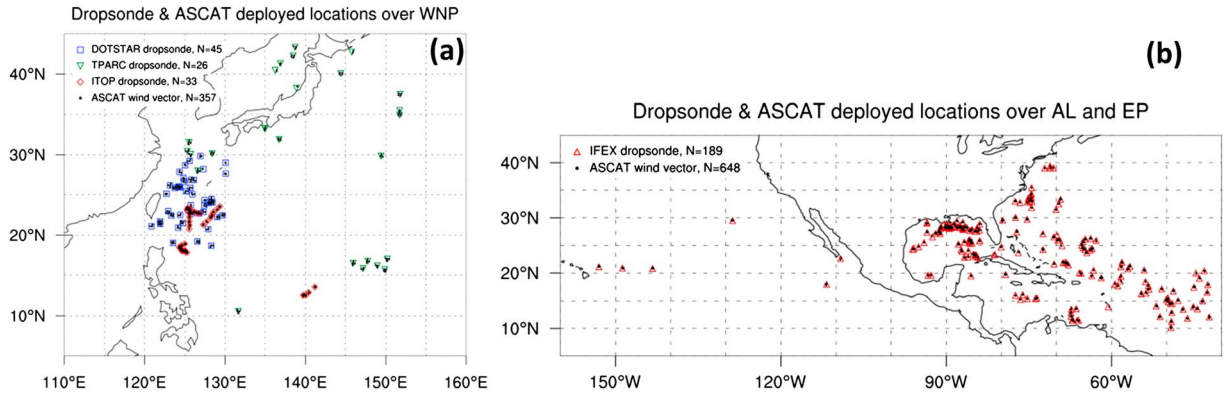

Figure 2. The locations of dropwindsonde and ASCAT-dropwindsonde matched samples over the (a) western North Pacific and (b) eastern Pacific and Atlantic. Black dots indicate the locations of ASCAT wind data, and other symbols represent the dropsonde locations from different research projects and field campaigns.

regression fit (following the method developed in *Chou et al.* [2010]). In this method, the U_{10} and M40 are defined and calculated by averaging wind vector between 8–12 m and 0–40 m of dropwindsonde measurement, respectively. In the data set used in this study, only 3516 (49%) dropwindsondes could be applied to calculate U_{10}, whereas 5233 (73%) dropwindsondes are available for the M40 calculation. Figure 1 shows the scatter diagram between M40 and U_{10} and the linear regression fit line calculated from dropwindsondes globally during 2007–2010. The corresponding best fit regression line between the M40 and U_{10} values is given by $U_{10\text{-}M40} = 0.961 \times M40 + 0.179$, with a correlation coefficient square (R^2) of 0.995. Note that the regression fit equation is further updated based on several thousand

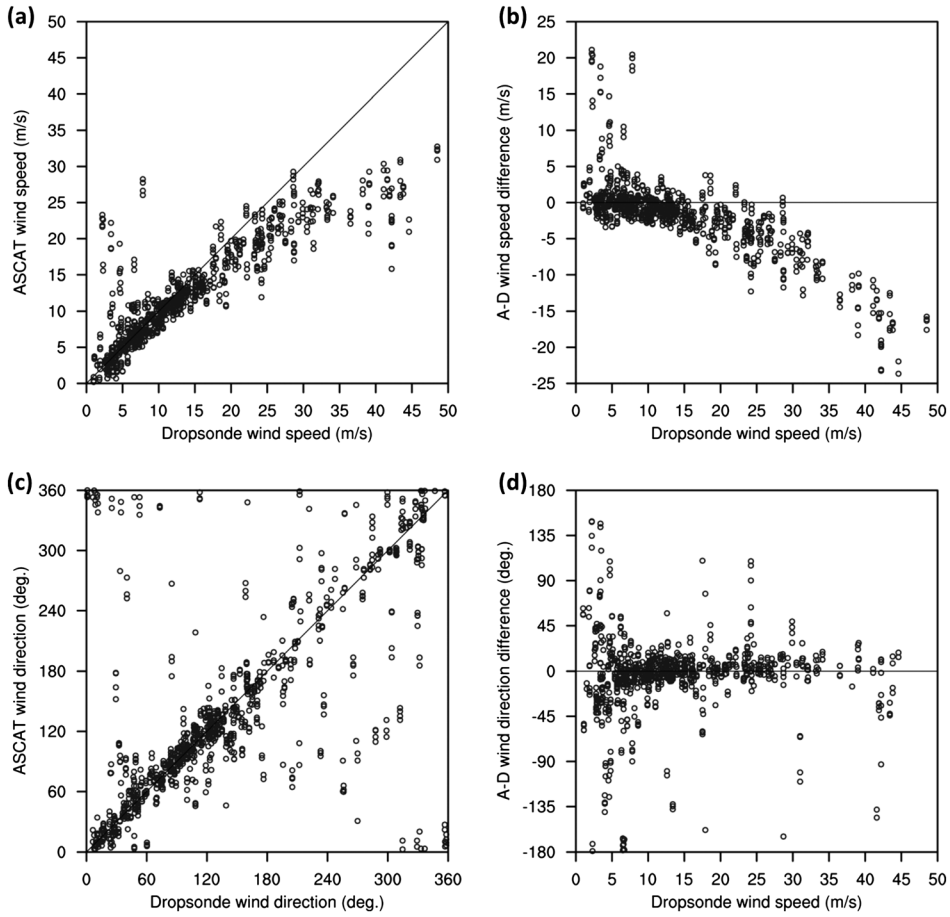

Figure 3. Scatter diagram of the (a) wind speed and (c) wind direction for ASCAT and dropwindsonde. Differences of (b) wind speed (ASCAT minus dropwindsonde) and (d) wind direction as a function of the dropwindsonde wind speed.

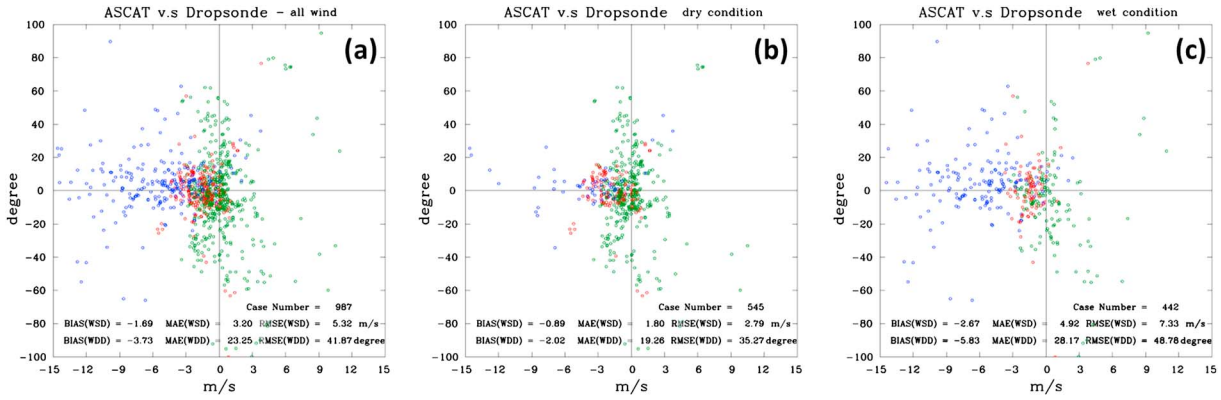

Figure 4. Scatter diagram of the wind speed and direction difference between the ASCAT surface wind and the estimated 10 m wind ($U_{10\text{-}M40}$). All matched samples (below 50 m s^{-1}) are sorted by wind speed and allocated ($U_{10\text{-}M40}$) to three different wind speed regimes. The samples with green, red, and blue markers represent those with weak wind (below 12 m s^{-1}), medium wind (12–18 m s^{-1}), and high wind (above 18 m s^{-1}), respectively. (a) All matched samples, (b) samples in unsaturated air condition, and (c) samples in saturated air condition.

dropwindsondes across the globe that directly measured the U_{10}. The original equation formulated in *Chou et al.* [2010] was $U_{10\text{-}M40} = 0.977 \times M40 + 0.056$; the difference between the above two regression formulas is insignificant.

[10] When the temporal and spatial differences between an ASCAT observation and a dropwindsonde observation are within 1 h and one wind vector cell distance, they are defined as matched samples. With this definition of collocation criterions, the differences between the observations are larger over high wind speed gradient regions, i.e., near the storm's inner core. As a result, the dropwindsondes that are located within the 500 km radius from the storm center are transformed to storm-relative coordinates at the time of the satellite overpass. Note that the ASCAT data with the finest resolution are downloaded in real time, and thus, the data resolution is 25 km from 2007 to 2009 and 12.5 km in 2010. Overall, there are 1005 matched samples obtained under the above criterion. Figure 2 shows the ASCAT-dropwindsonde matched samples analyzed in this study. Although the number of samples is not large enough to conduct a robust statistical analysis, these samples still provide some values to assess the accuracy of the ASCAT wind data.

[11] In this paper, the accuracy of rain-contaminated ASCAT wind data is also examined. Instead of using the rain-flagged information from the ASCAT wind products, the depth of accumulated saturated layers (DASL) of dropwindsonde is applied to identify if the wind vector cell is influenced by the rain or not. DASL is calculated based on the relative humidity measured by the dropwindsonde profile: DASL = Nsa × dz, where Nsat is the accumulated amount of layer where relative humidity exceeds 95.0%, and dz is the vertical resolution of the dropwindsonde profile. Higher DASL means that the dropwindsonde profile exhibits a thicker zone of saturated air, and lower DASL represents the dropwindsonde passing through the much clear sky condition. If the DASL value is larger than 200 m, the dropwindsonde is identified as a saturated condition dropwindsonde; otherwise, it is called an unsaturated condition dropwindsonde. Hereafter, the ASCAT-dropwindsonde matched samples can be categorized into saturated and unsaturated air samples according to the conditions of dropwindsondes. It should be noted that the threshold values of relative humidity and lengths of DASL on determining the saturated condition are also examined in section 3.2. It will be shown below that the main comparison results of ASCAT wind data accuracy are not significantly changed, and thus, it is reasonable to choose the 95% of relative humidity and 200 m of DASL as criterions in identifying the rain-contaminated ASCAT wind data.

3. Results

3.1. Overall Error Characteristics

[12] Because fewer matched samples between the ASCAT and dropwindsonde data are identified under the condition of higher wind speed, only 987 matched samples with ASCAT wind speed ranging between 0 and 50 m s^{-1} are analyzed. The scatterplot of the wind speed for dropwindsonde and ASCAT is shown in Figure 3a. The wind speeds derived from ASCAT are overestimated (underestimated) by dropwindsonde data in the condition of lower (higher) wind speed. The scatter diagram of wind speed difference between ASCAT and dropwindsonde as a function of dropwindsonde wind speed (Figure 3b) clearly shows the wind speed bias of the ASCAT data. The ASCAT wind data have a positive wind bias for wind speeds below 10 m s^{-1}, while a negative bias is found in wind speeds above 20 m s^{-1} as compared with dropwindsonde data. This result is consistent with the analyses in *Bentamy et al.* [2008], which compared the data between ASCAT and the buoys. The analyses of the ASCAT-buoy collocated samples indicate that the ASCAT wind data have positive (negative) bias in samples where wind speed is below 5 m s^{-1} (larger than 10 m s^{-1}), and a larger negative bias is found in higher wind speed. Note that Figure 3a shows a good number of samples in which the ASCAT wind speed is many times larger than the dropwindsonde wind speed. It is shown that those samples are located around the eye of the tropical cyclone, implying that the ASCAT data could not correctly retrieve the smaller wind speed value at this region. The difference of wind direction between ASCAT and dropwindsonde (Figures 3c and 3d) shows that a larger difference in wind direction occurs at lower wind speed (<10 m s^{-1}) and vice versa. Note that the wind direction error is a relative

Table 1. Comparisons of Wind Speed and Direction Between ASCAT and Dropwindsonde Data[a]

ASCAT Data	Bias	Mean Absolute Difference	RMS Difference	Number of Matching Samples
		Total		
All	−1.7 (−3.7)	3.2 (23.3)	5.3 (41.9)	987
Weak: below 12 m s^{-1}	0.7 (−5.3)	1.9 (28.8)	3.8 (48.6)	533
Medium: between 12 and 18 m s^{-1}	−1.6 (−2.8)	1.8 (13.8)	2.1 (28.0)	199
High: above 18 m s^{-1}	−6.9 (−1.2)	7.0 (19.1)	8.7 (35.2)	255
		Saturated Air Condition		
All	−2.7 (−5.8)	4.9 (28.2)	7.3 (48.8)	442
Weak: below 12 m s^{-1}	2.5 (−8.9)	3.4 (39.7)	6.3 (61.9)	163
Medium: between 12 and 18 m s^{-1}	−1.3 (−6.6)	1.6 (18.4)	1.8 (37.1)	88
High: above 18 m s^{-1}	−7.7 (−2.9)	7.8 (22.8)	9.4 (40.1)	191
		Unsaturated Air Condition		
All	−0.9 (−2.0)	1.8 (19.3)	2.8 (35.3)	545
Weak: below 12 m s^{-1}	−0.0 (−3.7)	1.2 (24.0)	1.8 (41.4)	370
Medium: between 12 and 18 m s^{-1}	−1.7 (0.2)	2.0 (10.1)	2.4 (17.7)	111
High: above 18 m s^{-1}	−4.4 (3.9)	4.7 (7.7)	6.2 (12.2)	64
		Total After Bias Correction		
All	−0.2	2.6	4.6	987
Weak: below 12 m s^{-1}	1.4	2.1	4.5	533
Medium: between 12 and 18 m s^{-1}	−0.6	1.4	1.8	199
High: above 18 m s^{-1}	−3.1	4.5	6.0	255

[a]Wind speed is given in m s^{-1}. Direction is given in degrees clockwise (value in parentheses).

quantity, which is dependent on wind speed. This appears as the main reason leading to large directional error for samples with smaller wind speed.

3.2. Error Characteristics in Different Wind Speed Regimes and Atmospheric Moisture Condition

[13] Figure 4a shows the scatter diagram of the wind speed and direction difference between the ASCAT and dropwindsonde data for all matched samples. To further examine the error characteristics, these samples are sorted into three different wind speed regimes by the magnitude of $U_{10\text{-}M40}$: weak wind speed (below 12 m s^{-1}), medium wind speed (between 12 and 18 m s^{-1}), and high wind speed (above 18 m s^{-1}). It is clearly shown that a large negative wind speed bias occurs in the high wind speed regime and a large wind direction difference appears in the weak wind speed regime, consistent with the result in Figure 3c. Furthermore, both wind speed and wind direction differences are relatively small in the medium wind speed regime.

[14] The error statistics are also calculated based on all available ASCAT-dropwindsonde matched samples. The ASCAT wind speed has a negative bias of −1.7 m s^{-1} calculated from all 987 matched samples. The wind speed bias is a positive value of 0.7 m s^{-1} in the weak wind speed regime, while it is a negative bias of −1.6 and −6.9 m s^{-1} in the medium and high wind speed regimes, respectively. The overall RMS difference of wind speed is 5.3 m s^{-1}. The RMS difference of wind speed in the weak, medium, and high wind speed regimes is 3.8, 2.1, and 8.7 m s^{-1}, respectively, indicating that the large RMS difference is mainly contributed by samples in the high wind speed regime. In wind direction comparisons, the overall wind direction bias is relatively small with a value of −3.7°, while the RMS difference is quite large with a value of 41.9°. The RMS difference of wind direction in the weak, medium, and high wind speed regimes is 48.6°, 28.0°, and 35.2°, respectively. Thus, the large RMS difference of wind direction is contributed by samples in the weak wind speed regime. The detailed error statistics are summarized in Table 1. Based on these ASCAT wind error statistics, it is found that the RMS differences of wind speed and direction in the medium wind speed regime are closer to the instrument design specifications for wind (±2 m s^{-1} in wind speed and ±20° in wind direction [*Pickett et al*., 2003]) as compared to those for the weak and high wind speed regimes.

[15] The influence of precipitation on wind retrieval due to the contamination of backscatter is examined by comparing the unsaturated and saturated ASCAT-dropwindsonde samples as shown in Figures 4b and 4c. In general, the scatter points in unsaturated samples are closer to the center of the figure than those in saturated samples, indicating that the wind difference between ASCAT and dropwindsonde in unsaturated air is smaller than that in saturated air. The RMS wind speed difference in unsaturated samples is 2.8 m s^{-1}, about 38% of the value in saturated samples. Meanwhile, the RMS wind direction difference in unsaturated samples is also reduced to a smaller value of 35.3° as compared to that in saturated samples. This result of larger errors in the rain-contaminated ASCAT wind data is generally consistent with the findings of *Hawkins and Black* [1983] and *Chou et al*. [2010], indicating that the accuracy of wind data retrieved from scatterometers is limited and is influenced by rain [*Weissman et al*., 2012].

[16] The sensitivity of different cutoff values of saturation and lengths of DASL on determining the rain-contaminated samples is shown in Table 2. It is clear that as DASL increases at the same cutoff value of saturation, the number of rain-contaminated samples is reduced since a thicker saturated layer is required to identify those samples. Furthermore, the magnitude of bias and RMS difference for wind speed in rain-contaminated samples also increases with the DASL value. This result indicates that the wind speed difference between ASCAT and dropwindsonde becomes larger in more saturated sounding profiles, implying that the ASCAT wind retrieval is obviously influenced by the saturation of air column and that the more negative bias of wind speed difference is found when the air column is more saturated. By comparing the wind speed differences among three cutoff values of saturation, much lower bias and RMS values between ASCAT and dropwindsonde unsaturated samples are found

Table 2. Comparisons of Samples That Are Sorted Under Different Cutoff Values of Saturation and Lengths of DASL for Saturated and Unsaturated Air Conditions[a]

DASL (m)	Saturated Air Condition			Unsaturated Air Condition		
	Number of Matching Samples	Bias	RMS Difference	Number of Matching Samples	Bias	RMS Difference
			Cutoff Value of Saturation (RH > 95)			
0	693	−2.13 (−4.25)	6.19 (46.95)	348	−0.87 (−2.75)	3.17 (30.38)
50	568	−2.29 (−5.53)	6.53 (46.93)	419	−0.86 (−1.28)	2.99 (33.82)
100	535	−2.36 (−6.15)	6.71 (47.90)	452	−0.89 (−0.86)	2.94 (33.34)
200	442	−2.67 (−5.83)	7.33 (48.78)	545	−0.89 (−2.02)	2.79 (35.27)
			Cutoff Value of Saturation (RH > 97)			
0	426	−2.51 (−3.63)	6.98 (42.64)	561	−1.06 (−3.80)	3.58 (41.27)
50	386	−2.67 (−3.29)	7.27 (43.50)	601	−1.05 (−4.01)	3.56 (40.78)
100	355	−2.84 (−3.44)	7.55 (45.25)	632	−1.04 (−3.89)	3.50 (39.84)
200	294	−3.41 (−6.53)	7.87 (45.29)	693	−0.96 (−2.54)	3.76 (40.32)
			Cutoff Value of Saturation (RH > 99)			
0	273	−2.90 (−6.57)	7.65 (46.94)	714	−1.22 (−2.64)	4.10 (39.76)
50	254	−3.09 (−6.83)	7.91 (48.22)	733	−1.20 (−2.65)	4.06 (39.42)
100	221	−3.69 (−5.72)	8.24 (43.43)	776	−1.11 (−3.15)	4.12 (41.40)
200	172	−3.87 (−5.67)	8.20 (44.63)	815	−1.23 (−3.32)	4.49 (41.26)

[a]DASL is calculated based on the dropwindsonde profile. Wind speed is given in $m\,s^{-1}$. Direction is given in degrees clockwise (value in parentheses).

in the classification of cutoff value of 95%. The bias difference between the saturated and unsaturated samples is also larger. These results indicate that using the cutoff value of 95% can reasonably classify the samples to saturated and unsaturated samples. Furthermore, the amounts in saturated and unsaturated samples are roughly the same when classified by a DASL of 200 m. As a result, considering the lower bias and RMS difference in unsaturated samples, the larger bias and RMS difference between saturated and unsaturated samples, as well as the equal amount of saturated and unsaturated samples, the 95% cutoff value of saturation and 200 m of DASL are chosen as the thresholds to categorize the samples into rain-contaminated and non-rain-contaminated groups in this study.

3.3. Error Characteristics in Different Portions of Tropical Cyclone or Dropwindsonde Sources

[17] The ASCAT wind error characteristic is further explored based on five different areas of TCs as demonstrated by the microwave brightness temperature image in Figure 5a. For a typical TC, the extent from the TC center to the outer environment is generally divided into five distinct areas from the axisymmetric viewpoint, i.e., the eye, eyewall, moat, rainband, and rain-free areas. The air is unsaturated in the eye, moat, and rain-free areas, while it is saturated in eyewall and rainband areas. In addition, the radius of the eye is empirically within 80 km, and the moat and eyewall regions are generally located near the inner core of the storm (about 200 km from the TC center). Therefore, the dropwindsonde data are classified into five groups corresponding to five TC areas, which are identified based on the wind speed, saturated condition of air, and the distance between the storm center and dropwindsonde observations.

[18] The distance between each dropwindsonde and the storm center is calculated based on the dropwindsonde splash location, while the location of the storm center at the dropwindsonde splashed time is interpolated from 6 hourly Joint Typhoon Warning Center or National Hurricane Center best track. Empirical criteria used to identify the five areas of a TC in this paper are as follows: eye (distance below 80 km, unsaturated air), eyewall (wind speed above $12\,m\,s^{-1}$, distance below 200 km, saturated air), moat (wind speed above $12\,m\,s^{-1}$, distance between 80 and 200 km, unsaturated air), rainband (wind speed above $12\,m\,s^{-1}$, distance between 200 and 500 km, saturated air), and rain-free (wind speed above $12\,m\,s^{-1}$, distance between 200 and 500 km, unsaturated air) areas. It should be noted that this partition has an arbitrary nature to it and the results have an uncertainty that stems from this. Furthermore, the best approach to classify five TC regions is likely using the orbit satellite microwave or aircraft radar imageries. However, since the dropwindsonde measurement does not always collocate with the orbit satellite measurement in both space and time, and the aircraft radar imagery is not easily accessible from the archive of aircraft measurement platform, therefore, the proposed empirical criteria are applied in this study. Figure 5b shows the locations of ASCAT-dropwindsonde samples of the five categories relative to the storm center. Overall, there are at least 20 samples in each group, and thus, the error statistic could still provide basic understanding of the accuracy of ASCAT wind data in different areas of the storm.

[19] Figure 6 shows the histogram of the wind difference between the ASCAT and dropwindsonde data in different areas of the TC. The ASCAT wind speeds are consistently underestimated in all the areas except in the eye area. The largest RMS difference of wind speed occurs around the eyewall area, and the largest RMS difference of wind direction appears in the eye area. The RMS differences of wind direction in moat, rainband, and rain-free areas are only about 12°, which are within the satellite's designed specifications for wind direction. The RMS differences of wind speed are between about 2.8 and $5.7\,m\,s^{-1}$, which exceed the satellite's designed specifications for wind speed.

[20] The ASCAT wind error characteristic could be further elaborated by sorting the dropwindsonde data based on different programs for data collection (i.e., DOTSTAR, IFEX, T-PARC, and ITOP; Figures 7a and 7b). It is found that the errors of both wind speed and direction for the matched samples from DOTSTAR and T-PARC are smaller than those from IFEX and ITOP. This error characteristic could be explained by the location of matched samples relative to the storm center and the magnitude of wind speed of the matched samples (Figures 7c and 7d). The wind speed of matched

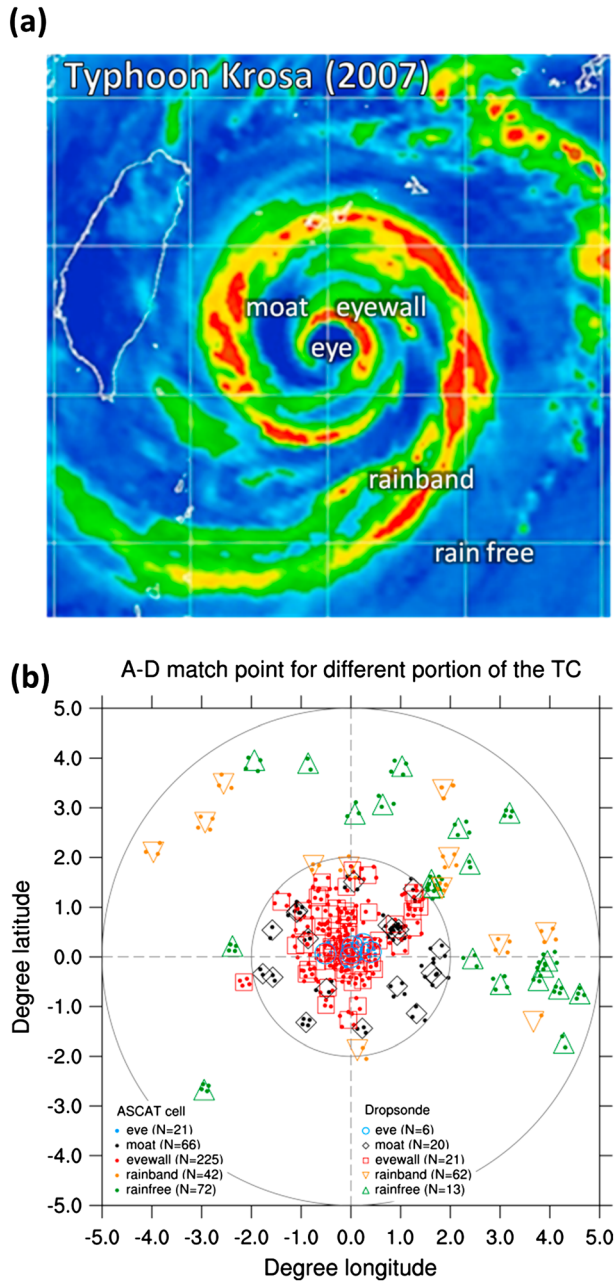

Figure 5. (a) The microwave image of 89 GHz brightness temperature at 1729 UTC on 5 October 2007 for Typhoon Krosa (from the Web site of the Naval Research Laboratory, Monterey, California) is shown in the schematic diagram for identifying the different components of the TC structure. (b) The locations of dropwindsonde and ASCAT-dropwindsonde matched samples relative to the TC center. Samples are classified into five different categories to represent the different portions of a tropical cyclone.

samples from DOTSTAR and T-PARC almost belongs to the lower wind regime (less than 20 m s^{-1}), and the distance between the storm center and most samples is more than 200 km. On the contrary, the wind speed of matched samples from IFEX and ITOP almost belongs to the higher wind regime (more than 20 m s^{-1}), and the distance between the storm center and most samples is less than 200 km.

3.4. ASCAT Wind Speed Bias Correction

[21] Based on the analyses in the previous subsection, the wind speed derived from ASCAT shows a systematic negative bias in the vicinity of the storm as compared with dropwindsonde data. In order to remove this negative wind speed bias, the original ASCAT wind speed is calculated and interpolated to dropwindsonde wind speed by a quadratic regression fit. Furthermore, to reduce the uncertainty of the signal attenuated by rain for retrieving scatterometer wind data, the interpolation is only calculated for 545 unsaturated ASCAT-dropwindsonde matched samples. It should be noted that since no significant bias is found in the wind direction comparison, the wind direction remains the same for this bias correction calculation.

[22] As shown in Figure 8a, the scatter diagram between the ASCAT wind speed (AWS) and dropwindsonde-estimated 10 m wind speed (DWS) indicates that the values of ASCAT wind data agree well with those of dropwindsonde wind observations. The corresponding best fit regression line between the ASCAT and dropwindsonde wind speeds is given by $DWS = 0.014 \times AWS^2 + 0.821 \times AWS + 0.961$, with a correlation coefficient square (R^2) of 0.851. The regression equation is applied for adjusting the ASCAT wind speed. Figures 8b and 8c show the scatterplots between the wind speed difference of the ASCAT-dropwindsonde sample and dropwindsonde wind speed for the unsaturated samples without and with ASCAT wind speed adjustment. It is evident that the negative

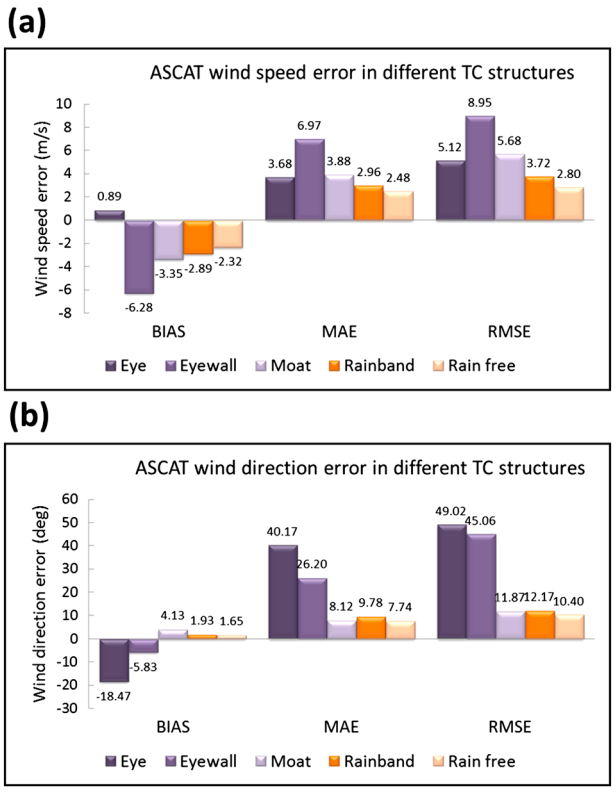

Figure 6. Histogram of the wind difference between the ASCAT and dropwindsonde data in terms of different components of TC structure: (a) wind speed and (b) wind direction. MAE represents the mean absolute difference; RMSE means the root-mean-squared difference.

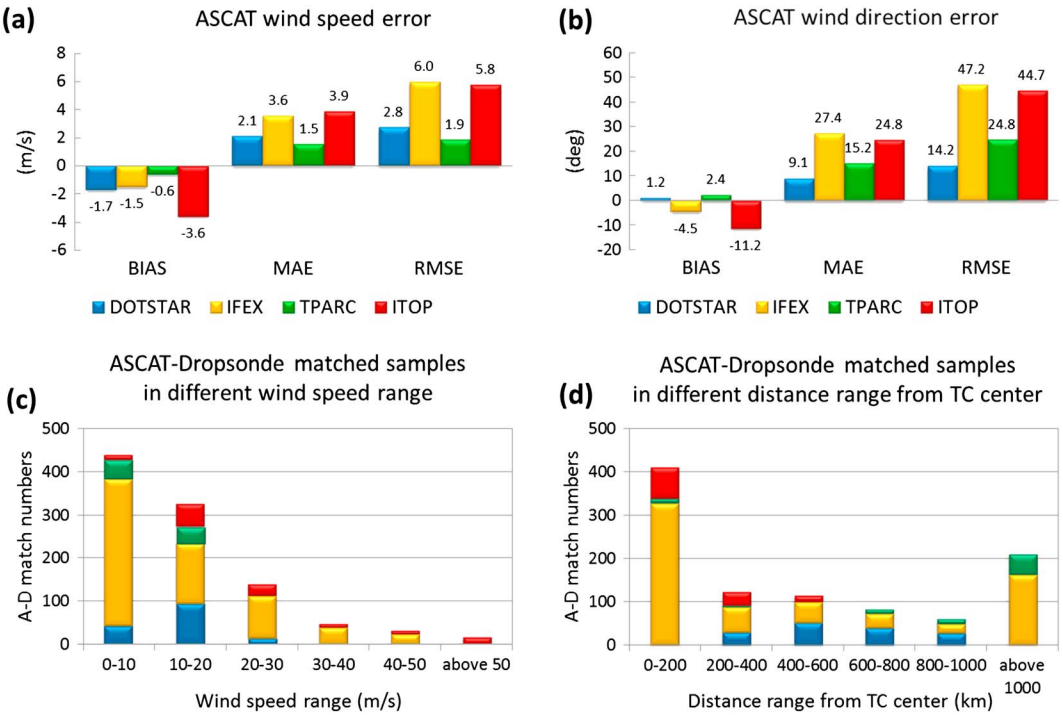

Figure 7. (a, b) Same as in Figure 6, but are for comparisons in which the dropwindsonde data are sorted by different projects. (c) The histogram of matched samples in different projects where the samples are sorted by the estimated 10 m surface wind speed. (d) Same as Figure 7c but samples are sorted by the distance from the storm center.

bias in the high wind speed regime is significantly reduced in the matched samples with ASCAT wind speed adjustment. Moreover, the bias is reduced from -0.89 to 0.01 m s^{-1}, and the RMS value is decreased from 2.79 to 2.49 m s^{-1} as well. Note that the sensitivity of linear and quadratic regression fit is also examined in this study. Results show that ASCAT data corrected by quadratic regression fit lead to much lower RMS values of wind speed difference and larger correlation coefficient square between both data. The quadratic regression fit is thus applied in the study (figure not shown).

[23] The error statistic of wind speed between the adjusted ASCAT and dropwindsonde for all the samples (including saturated and unsaturated samples) is also shown in Table 1. After the bias correction for all samples, the bias and RMS

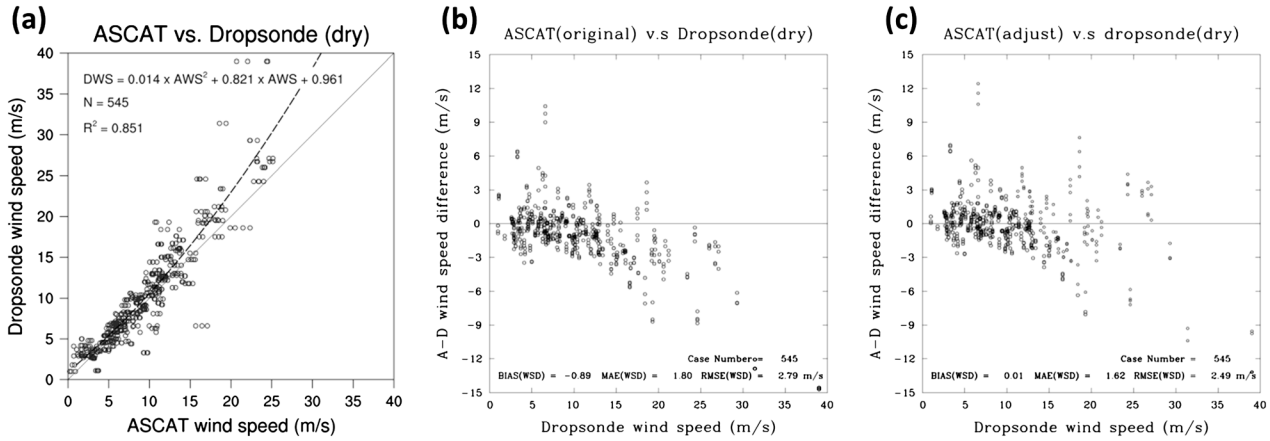

Figure 8. (a) Scatter diagram of the wind speed with the quadratic regression fit line for ASCAT wind speed and the dropwindsonde-estimated 10 m wind speed. (b) Relationship between the wind speed difference of ASCAT-dropwindsonde samples and the dropwindsonde-estimated 10 m wind speed. (c) Same as Figure 8b, but the ASCAT wind speed is adjusted by the proposed regression fit.

values are reduced from -1.7 to $-0.2\,m\,s^{-1}$ and from 5.3 to $4.6\,m\,s^{-1}$, respectively. Furthermore, among the three wind regimes, the bias and RMS values for the medium wind regime are only -0.6 and $1.8\,m\,s^{-1}$, which are under the satellite's designed specifications. However, the bias and RMS values in weak and high wind regimes still exceed the satellite's designed specifications. Since the error statistic of saturated samples is much larger than that of unsaturated samples, it cannot be efficiently removed by the proposed regression fit.

4. Discussion

[24] According to the previous assessments on validating the scatterometer wind data (most are QuikSCAT) against the buoy observations, the RMS difference between scatterometer and buoy wind data is under the satellite's designed specifications [*Freilich and Dunbar*, 1999; *Ebuchi et al*., 2002; *Pickett et al*., 2003; *Bentamy et al*., 2008]. However, since the wind speed of these scatterometer-buoy samples ranges between 3 and $15\,m\,s^{-1}$, the accuracy of scatterometer wind data under the condition of higher wind speed should be further examined. *Chou et al*. [2010] firstly validated the scatterometer wind data against GPS dropwindsonde observations, for the non-rain-flagged scatterometer-dropwindsonde samples, indicating that the RMS difference in wind speed and wind direction is $2.6\,m\,s^{-1}$ and 16.9°, respectively. Because more samples are analyzed in the high wind speed region around the storm, the errors are much larger than those obtained from the comparisons between the scatterometer and buoy wind data.

[25] In this study, following the work from *Chou et al*. [2010], the accuracy of ASCAT wind data is validated against the collocated GPS dropwindsonde observations. It is found that for the matched samples without the effect of rain contamination, the RMS difference of wind speed and wind direction is $2.8\,m\,s^{-1}$ and 35.3°, respectively. The RMS difference value in wind speed is almost equal to that analyzed in *Chou et al*. [2010], while the RMS value in wind direction doubles. The RMS difference in the samples where ASCAT is validated only against DOTSTAR dropwindsonde (as shown in Figures 7a and 7b) is $2.8\,m\,s^{-1}$ for wind speed and 14.2° for wind direction. These error statistics are nearly the same as the values in *Chou et al*. [2010], because the analysis is conducted on samples of weak wind speed around the eye area, thus leading to larger RMS wind direction difference. This comparison shows that the error statistic of ASCAT wind is strongly dependent on the magnitude of wind speed, which is highly variable in the inner core of the storm. Furthermore, the atmospheric moisture condition is also highly changeable around the storm; thus, the error values increase due to the heavy rain attenuation effect in the eyewall and rainband areas.

[26] The comparison between the ASCAT wind data and the dropwindsonde wind observations in this study shows that the ASCAT wind speed has a negative bias, the magnitude of which increases with the wind speed. The bias is $-6.9\,m\,s^{-1}$ for samples with wind speed larger than $18\,m\,s^{-1}$. This result is in agreement with the findings in *Bentamy et al*. [2008, 2012]. *Bentamy et al*. [2008] showed that the ASCAT wind has a slightly negative bias of about $0.5\,m\,s^{-1}$ in high wind speed conditions (above $10\,m\,s^{-1}$). The comparison between ASCAT and QuikSCAT indicates that for higher wind conditions, ASCAT has a low bias and the ASCAT underestimation with respect to QuikSCAT wind data becomes more significant when wind speed increases. *Bentamy et al*. [2012] conducted more collocated ASCAT-QuikSCAT samples for 13 months. The result showed that ASCAT wind speed is consistently lower than QuikSCAT for wind speed larger than $15\,m\,s^{-1}$ and revealed a clear dependence of the difference between ASCAT and QuikSCAT on ASCAT wind speed for wind speed between 15 and $25\,m\,s^{-1}$.

[27] It should be noted that because the sampling amount and range are different from those in *Bentamy et al*. [2008], the bias of ASCAT wind speed obtained in this study is much higher than the previous result. Nevertheless, based on our result and previous studies, the negative bias of ASCAT wind speed is robust. A systematic approach should be considered to correct the bias, such as methods proposed in this study, *Draper and Long* [2004], *Ricciardulli and Wentz* [2011], and *Bentamy et al*. [2012], for acquiring more accurate information from the ASCAT wind data.

5. Concluding Remarks

[28] In this study, the accuracy of ASCAT wind vectors in the environment of tropical cyclones (TCs) is evaluated through comparison with GPS dropwindsonde wind observations from 2007 to 2010. The data set used for the validation consists of several thousands of dropwindsonde atmospheric sounding profiles obtained in four different programs (DOTSTAR, NOAA/IFEX, T-PARC, and ITOP). The ASCAT orbit data are obtained from the KNMI website, and the resolution is 25 km between 2007 and 2009 and 12.5 km in 2010. Following the research by *Chou et al*. [2010], to obtain a larger sampling database, the surface-to-40 m averaged wind speed is calculated and interpolated to 10 m surface wind speed by a quadratic regression fit. When the temporal and spatial differences between an ASCAT observation and a dropwindsonde observation are within 1 h and one wind vector cell distance, they are defined as matched samples. The depth of accumulated saturated layers of dropwindsondes is applied to assess the rain attenuation issue of the ASCAT wind retrieval.

[29] In general, based on the calculation from 987 available ASCAT-dropwindsonde matched samples in which the wind speed ranges between 0 and $50\,m\,s^{-1}$, the bias and RMS differences of wind speed between ASCAT and dropwindsonde data are -1.7 and $5.3\,m\,s^{-1}$, respectively. Further analyses also indicate that large wind direction differences occur in the low wind speed regime (below $12\,m\,s^{-1}$), while large wind speed differences occur in the high wind speed regime (above $18\,m\,s^{-1}$). The accuracies of wind vector in weak and high wind speed regimes are significantly reduced for samples with the saturated condition of air, indicating that the accuracy of ASCAT wind retrieval is mainly limited by rain contamination. The wind vector in the medium wind speed regime (between 12 and $18\,m\,s^{-1}$) has much better quality, with a RMS difference of $2.1\,m\,s^{-1}$ for wind speed and 28.0° for wind direction, in good agreement with the satellite's designed specification.

[30] The ASCAT wind error characteristic could be further elaborated by sorting the data according to the areas in a TC and the dropwindsonde sources. For samples categorized by different areas of a TC, it is found that the largest RMS

difference of wind speed occurs around the eyewall area, and the highest RMS difference of wind direction appears in the eye area. The RMS differences of wind direction in moat, rainband, and rain-free areas are only about 12°, which is smaller than that in the eye and eyewall areas. Moreover, for samples sorted by different dropwindsonde sources, the error values of wind speed and direction are lower in dropwindsondes from DOTSTAR and T-PARC than those from IFEX and ITOP. These comparisons show that the error statistic of ASCAT wind is strongly dependent on the magnitude of wind speed, which is highly variable in the inner core of the storm. Furthermore, the saturated condition of the atmosphere is also highly changeable around the storm, and thus, the error values are higher for samples in the eyewall and rainband areas where heavy rain-contaminated effects exist.

[31] In this study, the wind speed retrieved from ASCAT shows a systematic negative bias in the vicinity of the storm, which is consistent with the findings in *Bentamy et al*. [2008, 2012]. In order to correct this negative bias in wind speed, the original ASCAT wind speed is calculated and interpolated to the dropwindsonde wind speed by a quadratic regression fit. After applying the bias correction to all matched samples, it is clearly shown that the negative bias in the high wind speed regime is reduced. Analyses also indicate that the bias and RMS values in the medium wind speed regime are only -0.6 and $1.8\,\mathrm{m\,s^{-1}}$, respectively, which are under the satellite's designed specifications. However, since the error statistic of saturated samples is much larger than that in unsaturated samples, the bias and RMS values in weak and high wind speed regimes still exceed the satellite's designed specifications. Nevertheless, results from these comparisons suggest that ASCAT wind speeds of around $12–18\,\mathrm{m\,s^{-1}}$ are more reliable and can be helpfully applied to determine the wind radius of 34 knot winds, a critical parameter in operational TC analyses.

[32] Since 2010, KNMI has released ASCAT data with the finest resolution of 12.5 km. The new product covers more data on coastal areas, and the wind quality is better with the wind speed bias below $0.5\,\mathrm{m\,s^{-1}}$ and wind component RMS above $2.0\,\mathrm{m\,s^{-1}}$ [*Verhoef et al*., 2012]. Since the ASCAT data with the finest resolution are archived in real time, the resolution of ASCAT data is different in the analyzed period (from 2007 to 2010). The issue of how the error statistic of ASCAT wind data is likely related to the data resolution needs to be addressed in follow-up studies by using more collocated ASCAT-dropwindsonde samples. Furthermore, the definition to identify the rain-contaminated data by the rain-flagged information of ASCAT wind products should be considered. In the future, the work will be extended to evaluate the wind accuracy within the environment of TCs for the Oceansat-2 scatterometer (OSCAT) which was launched in September 2009. The OSCAT is a Ku-band conically scanning scatterometer system designed and built by the India Space Research Organization/Space Applications Center. The accuracy of the OSCAT wind vector can be assessed by the same approach as in this study. In higher wind speed regions around TCs, there may be increases in temporal variability and spatial variability, i.e., gustiness and mesoscale structures, that render the comparison of point and area-averaged measurements difficult. Thus, comparison of the areal averaged scatterometer wind data and point dropwindsonde wind observations in the highly variable TC environment is another representative issue that needs to be addressed. A follow-up study is ongoing in which high spatial and temporal resolution data from numerical simulations of TCs are used to examine the representativeness and time-averaging issues of TC wind data. It is anticipated that this work will provide basic understanding on the accuracy of satellite-derived wind products, especially in TCs, for use in forecaster analysis and for initializing numerical forecast models. Moreover, the errors estimated here provide a benchmark for better scatterometers that will be designed in the future.

[33] **Acknowledgments.** The authors highly appreciate KNMI for providing the ASCAT data set and C.-H. Liu for conducting the preprocessing of the ASCAT data set. The work is supported by the National Science Council of Taiwan through grants NSC-100-2111-M-034-003 and NSC-101-2119-M-034-001, and the Central Weather Bureau of Taiwan through grants MOTC-CWB-101-M-04. The authors thank all DOTSTAR, T-PARC, ITOP, and NOAA/IFEX team members for their contribution to the observations.

References

Aberson, S. D. (2010), 10 years of hurricane synoptic surveillance (1997–2006), *Mon. Weather Rev.*, *138*, 1,536–1,549, doi:10.1175/2009MWR3090.1.

Aberson, S. D., and J. L. Franklin (1999), Impact on hurricane track and intensity forecasts of GPS dropwindsonde observations from the first-season flights of the NOAA Gulfstream-IV jet aircraft, *Bull. Am. Meteorol. Soc.*, *80*, 421–427, doi:10.1175/1520-0477(1999)080<0421:IOHTAI>2.0.CO;2.

Bentamy, A., D. Croize-Fillon, and C. Perigaud (2008), Characterization of ASCAT measurements based on buoy and QuikSCAT wind vector observations, *Ocean Sci.*, *4*, 265–274.

Bentamy, A., S. A. Grodsky, J. A. Carton, D. Croizé-Fillon, and B. Chapron (2012), Matching ASCAT and QuikSCAT winds, *J. Geophys. Res.*, *117*, C02011, doi:10.1029/2011JC007479.

Black, P. G., R. C. Gentry, V. J. Cardone, and J. D. Hawkins (1985), Seasat microwave wind and rain observations in severe tropical and midlatitude marine storms, in *Satellite Oceanic Remote Sensing*, Adv. in Geophysics, vol. *27*, edited by B. Saltzman, pp. 198–279, Academic Press, Inc., Orlando.

Brennan, M. J., C. C. Hennon, and R. D. Knabb (2009), The operational use of QuikSCAT ocean surface vector winds at the National Hurricane Center, *Weather Forecast.*, *24*, 621–645, doi:10.1175/2008WAF2222188.1.

Chen, S.-G., C.-C. Wu, J.-H. Chen, and K.-H. Chou (2011), Validation and interpretation of adjoint-derived sensitivity steering vector as targeted observation guidance, *Mon. Weather Rev.*, *139*, 1,608–1,625, doi:10.1175/2011MWR3490.1.

Chou, K.-H., C.-C. Wu, P.-H. Lin, and S. Majumdar (2010), Validation of QuikSCAT wind vectors by dropwindsonde data from Dropwindsonde Observations for Typhoon Surveillance Near the Taiwan Region (DOTSTAR), *J. Geophys. Res.*, *115*, D02109, doi:10.1029/2009JD012131.

Chou, K.-H., C.-C. Wu, P.-H. Lin, S. D. Aberson, M. Weissmann, F. Harnisch, and T. Nakazawa (2011), The impact of dropwindsonde observations on typhoon track forecasts in DOTSTAR and T-PARC, *Mon. Weather Rev.*, *139*, 1,728–1,743, doi:10.1175/2010MWR3582.1.

D'Asaro, E., et al. (2011), Typhoon-ocean interaction in the western North Pacific: Part 1, *Oceanography*, *24*(4), 24–31, doi:10.5670/oceanog.2011.91.

Draper, D. W., and D. G. Long (2004), Evaluating the effect of rain on SeaWinds scatterometer measurements, *J. Geophys. Res.*, *109*, C02005, doi:10.1029/2002JC001741.

Ebuchi, N., H. C. Graber, and M. J. Caruso (2002), Evaluation of wind vectors observed by QuikSCAT/SeaWinds using ocean buoy data, *J. Atmos. Oceanic Technol.*, *19*, 2,049–2,062, doi:10.1175/1520-0426(2002)019<2049:EOWVOB>2.0.CO;2.

Elsberry, R. L., and P. A. Harr (2008), Tropical cyclone structure (TCS08) field experiment science basis, observational platforms, and strategy, *Asia Pacific J. Atmos. Sci.*, *44*, 209–231.

Freilich, M. H., and R. S. Dunbar (1999), The accuracy of the NSCAT vector winds: Comparisons with National Data Buoy Center buoys, *J. Geophys. Res.*, *104*, 11,231–11,246, doi:10.1029/1998JC900091.

Hawkins, J. D., and P. G. Black (1983), Seasat scatterometer detection of gale force winds near tropical cyclones, *J. Geophys. Res.*, *88*, 1,674–1,682, doi:10.1029/JC088iC03p01674.

Hawkins, J., and C. Velden (2011), Supporting meteorological field experiment missions and postmission analysis with satellite digital data and products, *Bull. Am. Meteorol. Soc.*, *92*, 1,009–1,022, doi:10.1175/2011BAMS3138.1.

Hersbach, H., A. Stoffelen, and S. de Haan (2007), An improved C-band scatterometer ocean geophysical model function: CMOD5, *J. Geophys. Res.*, *112*, C03006, doi:10.1029/2006JC003743.

Hock, T. F., and J. L. Franklin (1999), The NCAR GPS dropwindsonde, *Bull. Am. Meteorol. Soc.*, *80*, 407–420, doi:10.1175/1520-0477(1999)080<0407:TNGD>2.0.CO;2.

Huang, Y.-H., M. T. Montgomery, and C.-C. Wu (2012), Concentric eyewall formation in Typhoon Sinlaku (2008). Part II: Axisymmetric dynamical processes, *J. Atmos. Sci.*, *69*, 662–674, doi:10.1175/JAS-D-11-0114.1.

Parsons, D., P. Harr, T. Nakazawa, S. Jones, and M. Weissmann (2008), An overview of the THORPEX-Pacific Asian Regional Campaign (T-PARC) during August-September 2008. Extended Abstracts, 28th Conf. on Hurricanes and Tropical Meteorology, Orlando, FL, AMS, 1–6.

Pickett, M. H., W. Tang, L. K. Rosenfeld, and C. H. Wash (2003), QuikSCAT satellite comparison with nearshore buoy wind data off the U.S. west coast, *J. Atmos. Oceanic Technol.*, *20*, 1,869–1,879, doi:10.1175/1520-0426(2003)020<1869:QSCWNB>2.0.CO;2.

Ricciardulli, L., and F. Wentz (2011), Reprocessed QuikSCAT (V04) Wind Vectors with Ku-2011 Geophysical Model Function, Remote Sensing System Technical Report 043011. [Available at http://www.ssmi.com/.]

Rogers, R. F., et al. (2006), The Intensity Forecasting Experiment: A NOAA multiyear field program for improving tropical cyclone intensity forecasts, *Bull. Am. Meteorol. Soc.*, *87*, 1,523–1,537, doi:10.1175/BAMS-87-11-1523.

Rogers, R. F., et al. (2013), NOAA's Hurricane Intensity Forecasting Experiment: A progress report, *Bull. Am. Meteorol. Soc.*, *94*, 859–882, doi:10.1175/BAMS-D-12-00089.1.

Verhoef, A., M. Portabella, A. Stoffelen, and H. Hersbach (2008), CMOD5.n—The CMOD5 GMF for neutral winds, OSI SAF report, SAF/OSI/CDOP/KNMI/TEC/TN/165. [Available at http://www.knmi.nl/scatterometer/publications/.]

Verhoef, A., M. Portabella, and A. Stoffelen (2012), High-resolution ASCAT scatterometer winds near the coast, *IEEE Trans. Geosci. Remote Sens.*, *50*(7), 2,481–2,487, doi:10.1109/TGRS.2011.2175001.

Weissman, D. E., and M. A. Bourassa (2011), The influence of rainfall upon scatterometer estimates for sea surface stress and boundary layer parameterization models within tropical cyclone environments, *IEEE Trans. Geosci. Remote Sens.*, *49*(12), 4,805–4,814, doi:10.1109/TGRS.2011.2170842.

Weissman, D. E., B. W. Stiles, S. M. Hristova-Veleva, D. G. Long, D. K. Smith, K. A. Hilburn, and W. L. Jones (2012), Challenges to satellite sensors of ocean winds: Addressing precipitation effects, *J. Atmos. Oceanic Technol.*, *29*, 356–374, doi:10.1175/JTECH-D-11-00054.1.

Wu, C.-C., et al. (2005), Dropwindsonde observations for typhoon surveillance near the Taiwan region (DOTSTAR): An overview, *Bull. Am. Meteorol. Soc.*, *86*, 787–790, doi:10.1175/BAMS-86-6-787.

Wu, C.-C., K.-H. Chou, P.-H. Lin, S. D. Aberson, M. S. Peng, and T. Nakazawa (2007), The impact of dropwindsonde data on typhoon track forecasts in DOTSTAR, *Weather Forecast.*, *22*, 1,157–1,176, doi:10.1175/2007WAF2006062.1.

Wu, C.-C., Y.-H. Huang, and G.-Y. Lien (2012a), Concentric eyewall formation in Typhoon Sinlaku (2008). Part I: Assimilation of T-PARC data based on the Ensemble Kalman Filter (EnKF), *Mon. Weather Rev.*, *140*, 506–527, doi:10.1175/MWR-D-11-00057.1.

Wu, C.-C., S.-G. Chen, C.-C. Yang, P.-H. Lin, and S. D. Aberson (2012b), Potential vorticity diagnosis of the factors affecting the track of Typhoon Sinlaku (2008) and the impact from dropwindsonde data during T-PARC, *Mon. Weather Rev.*, *140*, 2,670–2,688, doi:10.1175/MWR-D-11-00229.1.